Constructing hydrogen bond based melam/WO_3 heterojunction with enhanced visible-light photocatalytic activity

Zhengyuan Jin,[a,b] Qitao Zhang,[b] Liang Hu,[a] Jiaqi Chen,[a] Xing Cheng,[c] Yu-Jia Zeng, [a,d,*] Shuangchen Ruan,[a,**] and Teruhisa Ohno[b]

[a] Shenzhen Key Laboratory of Laser Engineering, College of Optoelectronic Engineering, Shenzhen University, Shenzhen, 518060, P. R. China

[b] Department of Applied Chemistry, Faculty of Engineering, Kyushu Institute of Technology, 1-1 Sensuicho, Tobata, Kitakyushu 804-8550, Japan

[c] Department of Materials Science and Engineering, South University of Science and Technology of China (SUSTC)

[d] State Key Laboratory of Silicon Materials, Department of Materials Science and Engineering, Zhejiang University, Hangzhou 310027, P. R. China.

Corresponding Author

[*]E-mail: yjzeng@szu.edu.cn. (Y.-J.Z.)

[**]E-mail: scruan@szu.edu.cn. (S.-C.R.)

Abstract: Hydrogen bond based visible-light-response heterojunction photocatalyst Melam/WO_3 (MW) has been fabricated for the first time by facile planetary milling treatment. Fourier transform infrared spectroscopy (FTIR) and Thermogravimetric (TG) analysis reveal the formation of hydrogen bonds (NH···O) between melam and WO_3. As compared to WO_3, the MW not only complete decomposes acetaldehyde, but also shows 10 times and 12 times higher photocatalytic activity for photo-degradation of 2-propanol and photo-generation of H_2O_2, respectively, under the visible-light irradiation. X-ray photoelectron spectroscopy suggests that the potential difference between N and O ($N^+H\cdots O^-$) in the heterojunction provides the driving force for the charge transfer from WO_3 to melam. Furthermore, hydrogen bonds offer an ultrafast electron pathway for heterojunction. This study demonstrates that hydrogen bond based heterojunction could be a promising approach for developing a new photocatalyst with efficient visible-light photocatalytic activity.

Graphical abstract

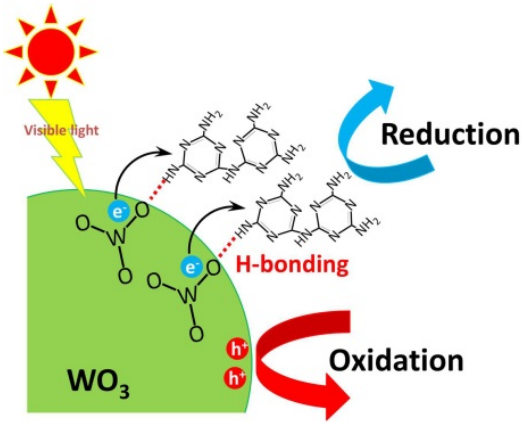

Highlights

- A hydrogen bond based heterojunction photocatalyst is fabricated by planetary milling treatment.
- The photocatalytic performance for CH_3CHO and $(CH_3)_2CHOH$ degradation is evaluated.
- The photocatalytic performance for H_2O_2 generation is detected.
- Melam/WO_3 shows much higher activity than bulk WO_3.
- A mechanism based on hydrogen bond of heterojunction photocatalyst is proposed.

Keywords: Photocatalysis, Melam, WO_3, Planetary mill, Hydrogen bond

1. Introduction

Along with the energy crisis and the increased environmental pollution, photocatalytic materials have inspired worldwide research efforts [1]. In addition to TiO_2, a firstly used and well studies photocatalyst [2], various new photocatalysts have been developed with higher photocatalytic activity in the water splitting, carbon dioxide fixation/conversion, waste-water purification and related pollutions degradation [3-6]. Among them, WO_3 is considered as one of the most promising photocatalyst not only because of a medium band gap of 2.4 ~ 2.7 eV but also the deep valence band (+3.1 V vs SHE). However, the conduction band of WO_3 (+0.5 V vs SHE) is not positive enough for single-electron reduction of oxygen [E^0 (O_2/$^{\bullet}O_2^-$) = -0.33 V or E^0 (O_2/$^{\bullet}HO_2$) = -0.05 V vs SHE]. Only two-electron reduction [E^0 (O_2/H_2O_2) = +0.68 V vs. SHE] or four-electron reduction [E^0 (O_2/H_2O) = +1.23 V vs. SHE] is possible to consume electrons [7-9]. As a result, WO_3 presents a high electron-hole recombination rate, which limits its application as a photocatalyst.

It has been reported that loading noble metals can solve the aforementioned issue. Pt-WO_3, Pd-WO_3 and PtPb-WO_3 exhibit high photocatalytic activity for the decomposition of aliphatic compounds [10-12]. This is because the noble metal on the surface accelerates the multi-electron reduction of dioxygen, which decreases the electron-hole recombination rate of WO_3. However, the cost of noble metals sets the limits to this type of materials from practical applications. On the other hand, constructing Z-scheme photocatalysis system with other photocatalysts has been proposed to solve the problems of WO_3 [13], such as CdS/WO_3, $CaFe_2O_4$/WO_3 and AgI/WO_3 [14-16]. In our previous study, the g-C_3N_4/WO_3 composite showed high photocatalytic activity for acetaldehyde decomposition under the visible-light irradiation as a result of Z-scheme charge transfer [17]. However, with longer irradiation time the activity of samples decreases, which is

probably due to the fact that not all g-C_3N_4 and WO_3 are connected tightly to guarantee an efficient Z-scheme mechanism. Further looking into the connection between g-C_3N_4 with WO_3, we found an exciting phenomenon that the heterojunction obtained by facile planetary milling treatment of WO_3 and melamine (a precursor of g-C_3N_4 [18]) in water showed extremely high photocatalytic activity for acetaldehyde decomposition under the visible-light irradiation, in which hydrogen bonds are believed to play a vital role. Note that melam ($[C_3N_3(NH_2)_2]_2NH$) is a s-triazine-based dimer (shown in Scheme S1) [19]. As part of sp^2-hybridized carbon nitride family, melam is expected to show promising properties for photocatalysis like another member of g-C_3N_4 [20], which is one of the attractive photocatalyst recently [21]. However, fabricating pure melam is extremely difficult as it is a short lived intermediate in the synthesis process of g-C_3N_4 [22, 23].

In this study, visible-light photocatalytic activities of as prepared melam/WO_3 (MW) heterojunction are studied by the decomposition of acetaldehyde and 2-propanol (oxidation) as well as by the photo-generation of H_2O_2 (reduction). Moreover, charge transfer mechanism based on hydrogen bond has been discussed in detail.

2. Experiment Section

2.1 Materials

Melamine (Wako Pure Chemical Industries, Ltd.) and WO_3 (Kojundo Chemical Laboratory Co.) were used as starting materials without further treatment. Deionized water (18.4 MΩ, PURELAB flex3 water systems) was used in the whole experiments.

2.2 Preparation of melam/WO_3 (MW)

Five hundred milligram of WO_3 and 500 mg of melamine powders and 20 mL of deionized water were added to a 50 mL agate bowl containing 50 g of YSZ grinding beads (Nikkato Co., = 0.6 mm). Then the agate bowl was put on planetary mill instrument (Fritsch Japan Co., Planetary Micro Mill pulverisette 7) and the planetary mill instrument was operated at 750 r m^{-1} for 20 min. After removing the beads by screening, the sample was separated by filtration, washed with deionized water several times, and dried in a vacuum drying oven at 333 K overnight. As a reference, each sample, i.e., original melamine and WO_3 was treated by the same procedure.

2.3. Noble-Metal loading by photo-deposition

Photo-deposition of Pt was carried out to determine the reduction sites of melam/WO_3 (MW) nanocomposite particles [24]. For Pt-MW preparation, 200 mL aqueous MW suspension containing 0.5 g MW, 5 mL methanol, and 1 mM hexachloroplatinic acid ($H_2PtCl_6 \cdot 6H_2O$) was irradiated for 24 hours with a 500 W Hg lamp (USHIO Co. Ltd., SX-UI501HQ), and the light intensity was 30 mW cm^{-2}. N_2 gas was vigorously purged through the suspension prior to UV irradiation. After irradiation, the color of the powder changed from green to gray, and the suspension was centrifuged and washed with distilled water and then collected as powder after drying for 3 hours at 60 °C under the reduced pressure.

2.4. Characterization

Crystal structure of the obtained samples were characterized by X-ray diffractometer (XRD, Rigaku, MiniFlex II) with CuKα radiation (λ = 1.5405Å). The morphology was imaged by field emission scanning electron microscopy (FE-SEM; JEOL, JSM-6701FONO) and transmission electron microscopy (TEM, HR-TEM; Tecnai F30 S-TWIN). UV-vis diffuse reflectance spectra (UV-vis DRS) were measured using a UV-vis spectrophotometer (Shimadzu, UV-2600)

equipped with an integrating sphere unit (Shimadzu, ISR-2600 Plus). Functional group vibrations were confirmed by using a Fourier transform infrared spectrometer (FTIR, JASCO, FT / IR 4200) with a diffuse reflectance accessory (JASCO, DR-81). Thermogravimetric (TG) analysis was measured by using (Rigaku TG・TDA-8120H). Specific surface area (S_{BET}) and pore size/volume were determined with a surface area analyser (Quantachrome, Nova 4200e) from the Brunauer-Emmett-Teller (BET) and Barrett-Joyner-Halenda (BJH) theory. Surface chemical states were investigated by X-ray photoelectron spectroscopy (XPS) measurement with Thermo Scientific ESCALAB 250Xi system by Al Ka radiation and adventitious C1s peak (284.6eV) as the reference. Fluorescence spectrophotometer (Edinburgh Instruments FLS-920; 405 nm as incident light source) was used to determine photoluminescence and the time-resolved fluorescence decay.

2.5. Photocatalytic measurement

2.5.1. Photo-decomposition of acetaldehyde and 2-propanol

Before evaluation of the photocatalytic activity, each sample was irradiated with UV light using black light (UVP, XX-15BLB) in order to remove impurities contaminant on the sample. The photocatalytic activity of MW heterojunction was evaluated by CO_2 liberation from photocatalytic mineralization of acetaldehyde. One hundred milligrams of the powder, which has complete extinction of incident radiation, was spread on the bottom of glass dish, and the glass dish was placed in a Tedlar bag (AS ONE Co. Ltd.). Then 125 cm^3 artificial air, which contains of 500 ppm of acetaldehyde was injected into the bag. Photoirradiation was performed at room temperature after the acetaldehyde had reached the adsorption equilibrium (after 2 hours). A 435 nm light emitting diodes (LED, Epitex, L435-30M32L) were used as a light source, and its intensity was 3.0 mW cm^{-2}. The concentration of CO_2 was collected by on-line gas

chromatography (Agilent Technologies, 3000A Micro-GC, TCD detector) equipped with OV1 and PLOT-Q columns as a function of irradiation time.

For the measurement of action spectra, acetaldehyde decomposition was proceeded under four different light-emitting diodes (Nichia NCCU033B, Epitex L435-30M32L, Lumileds LXHL-LB3C and Lumileds LXHL-MM1D), which emitted light at wavelengths of ca. 365 nm, 435 nm, 470 nm and 530 nm, respectively. The catalyst was irradiated for 4 hours, the average of irradiation was determined to be 3 mW cm^{-2}, and the irradiation area was 6.15 cm^3. The number of incident photons were calculated by equation (1), and the apparent quantum efficiency (QE) were calculated by the equation (2).

$$Number\ of\ incident\ photons = \frac{E\lambda}{hc} \quad (1)$$

$$QE = \frac{\text{number of reacted electrons}}{\text{number of incident photons}} \text{ x } 100\% = \frac{\text{number of evolved CO2 molecules x 5}}{\text{number of incident photons}} \text{ x } 100\% \quad (2)$$

The Photo-decomposition of 2-propanol was evaluated by same procedure with acetaldehyde, except contain 500 ppm of 2-propanol in a Tedlar bag.

2.5.2 Photocatalytic reduction of O_2 to H_2O_2

The amount of H_2O_2 produced was analyzed according to the literature with a slight modification [25]. Ten milligrams of photocatalyst suspended in 10 mL of water was placed Pyrex test tube (30 mL). A 435-nm LED was used as a light source, and its intensity was 3.0 mW cm^{-2}. Syringe was used to remove 2 mL of the solution and PVDF filter (Millex®W) was used to separate photocatalyst from solution. 1 mL of 0.1 mol L^{-1} potassium hydrogen phthalate ($C_8H_5KO_4$)

aqueous solution and 1 mL of 0.4 mol L^{-1} potassium iodide (KI) aqueous solution were added to obtained solution, which was then kept for 30 minutes. The H_2O_2 molecules reacted with iodide anions (I^-) under acidic conditions ($H_2O_2 + 3I^- + 2H^+ \rightarrow I_3^- + 2H_2O$) to produce triiodide anions (I_3^-) possessing a strong absorption at around 350 nm. The amount of I_3^- was determined by means of UV-vis spectroscopy on the basis of the absorbance at 350 nm, from which the amount of H_2O_2 produced during each reaction was estimated.

2.5.3 Photoelectrochemical measurements

The sample was fabricated on FTO substrates by an electrophoresis method. 10 mg of the sample and a spot of iodine were ultrasonically dispersed in 20 ml acetone solution. Two FTO conducting glasses were placed in the solution as anode and cathode. A bias of 15 V was applied between the two electrodes using a direct current power supply for 3 min (3 times). Sample loaded FTO was then dried.

Linear sweep voltammetry and chronoamperometry measurements were carried out by using an automatic polarization system (HSV-100, Hokuto Denko Co.) with a three electrode system, in which the prepared electrode, a Pt and a Ag/AgCl electrode were used as the working electrode, counter electrode and reference electrode, respectively. The electrolyte used was 0.5 M Na_2SO_4 solution. The light source used was an AM 1.5 G solar-simulated system (PEC-L15, Peccell Tech., Inc.). The light intensity of the solar-simulated light was adjusted to 100 mW cm^{-2} by utilizing a thermopile power meter (ORION-TH). The linear sweep voltammogram (LSV) was scanned in the anodic direction at a scan rate of 10 mV s^{-1}.

3. Results and discussion

Fig. 1a shows X-ray diffraction (XRD) patterns of WO_3, MW and melamine. MW contains peaks which belong to monoclinic structure of WO_3 (JCPDS 43-1035) while no peak related to melamine was detected in the sample. Moreover, peaks at 7.6, 8.7, 10.5, 12.5, and 15.3 degree, which can be indexed as melam, are evident in the MW sample [19, 23]. XRD patterns suggest that the melam is formed by the condensation of melamine. As a result, the MW heterojunction has been obtained by the planetary milling treatment.

To better understand the inter-connection between WO_3 and melam, functional groups of the WO_3, MW and melamine are analyzed by FTIR. As shown in Fig. 1b, the characteristic IR spectrum of WO_3 shows peaks at 1029 and 1044 cm^{-1}, which can be attributed to stretching O-W-O modes of the bridging oxygens [26]. After planetary milling treatment the O-W-O bond of the MW shifts to the lower frequency of 969 and 988 cm^{-1}, which is due to the strong interaction between the WO_3 and melam. On the other hand, the narrow peak at 3476 cm^{-1} originating from N-H bond in melamine changes to a broad peak around 3396 cm^{-1} in the MW. Moreover, two broad peaks at around 2690 cm^{-1} and 2850 cm^{-1} appear in the MW. The shift of O-W-O peaks and the appearance of these broad peaks are presumably attributed to the presence of N-H···O linkages between WO_3 and melam [27, 28]. Note that there also appear 1118, 1163, 1207, and 1352 cm^{-1} peaks in the MW, which can be attributed to C-NH-C units and is another evidence for the forming of melam [19, 23].

TG analysis with a heating rate of 10 °C min^{-1} was carried out to confirm the presence of N-H···O hydrogen bonds as shown in Fig. S2. It can be found that the first weight loss (~7 wt%) occurs at around 290 °C, which can be attributed to loss of water and the sublimation of free melamine molecules. The second weight loss (~8.5 wt%) occurs at around 415 °C, which is

higher than the sublimation temperature of melam (370 °C). The improved stability is due to the presence of the inter-connection hydrogen bonds between melam and WO_3 [29].

The XRD patterns of melamine and WO_3 after planetary milling treatment are also shown in Fig. S3. No melam-related phase is detected in PM-melamine (planetary milling treated melamine). As compared to the WO_3, the PM-WO_3 (planetary milling treated WO_3) shows extra peaks at 12.8 and 16.5 degree, which are identified as $H_2WO_4{\cdot}H_2O$ (JCPDS 18-1420) and $WO_3{\cdot}H_2O$ (JCPDS 43-0679), respectively. Moreover, MW cannot be obtained by the manual grinding (data not shown). It should be noted that no peaks of $H_2WO_4{\cdot}H_2O$ or $WO_3{\cdot}H_2O$ has been observed in the MW sample. These results suggest that WO_3 and the planetary milling treatment play a key role in the synthesis process. The route of synthesizing melam/WO_3 by planetary milling treatment is illustrated in Fig. 2. Firstly, O in the WO_3 is activated by the high temperature, which results from planetary milling treatment. Secondly, the activated O is connected with melamine by the hydrogen bonds. Finally, melam is formed by the condensation of melamine and the MW heterojunction is thus obtained.

The photocatalytic activities of the prepared samples were evaluated by CO_2 liberation from photodecomposition of acetaldehyde. Fig. 3a shows the time course of CO_2 generation over the WO_3 and MW photocatalysts under the visible-light irradiation (LED 435 nm). WO_3 only shows a high CO_2 liberation rate at the initial photo irradiation. However, the rate stops after longer photo irradiation before reaching 1000 ppm (ca. 500 ppm) of CO_2 generation. As expected, WO_3 can only decompose acetaldehyde to intermediates (formaldehyde and/or formic acid) with CO_2 liberation (Fig. S3) and cannot completely decompose these intermediates without efficient electron consumption [30]. On the other hand, MW shows extremely high CO_2 liberation rate at

the initial photo irradiation, which is about 3 times higher than WO_3. Moreover, MW shows no saturation tendency of CO_2 liberation as the irradiation time and complete decomposes acetaldehyde into CO_2 (ca. 1000 ppm). In addition, action spectra of MW were measured by acetaldehyde decomposition under four different light sources. The results showed in Fig. 3b as function of incident light wavelength with UV-vis absorption spectra of MW. The quantum efficiency (QE) decreases with the increasing wavelength and the onset of action spectrum coincides with the absorption edge of the MW composite, which suggests the reaction proceeds by the catalyst under photoirradiation.

Fig. 3c shows the time course of acetone generation over the WO_3 and the MW from photodecomposition of 2-propanol. WO_3 shows a low acetone generation rate (38.32 ppm after 12 hours irradiation) due to the low efficiency of the multi-electron reduction of O_2 on WO_3. On the other hand, MW not only shows 10 times (384.6 ppm after 12 hours irradiation) higher acetone generation rate than WO_3, but also continuous degradation of acetone to CO_2 (Figure S4). These significantly enhanced photocatalytic activities are due to the low charge recombination rate in the MW heterojunction.

H_2O_2 is the major product of O_2 reduction process [$O_2 + 2H^+ + 2e^- \rightarrow H_2O_2$, E^0 (O_2/H_2O_2) = +0.68 V vs. SHE] on WO_3 [25]. The photocatalytic reaction in water to generate H_2O_2 during O_2 reduction using the WO_3 and the MW is evaluated (air atmosphere). From the results of Fig. S5, the time courses for H_2O_2 production in water are plotted in Fig. 3d. MW produces 36.73 μM of H_2O_2, which is 12 times higher than 3.23 μM of WO_3 after 24-hour visible-light (LED-435 nm, 3 mW cm^{-2}) irradiation. Along with the H_2O_2 generation no H_2 can be detected (data is not shown), which indicates H_2O_2 is the only reduction product during the photocatalytic process. The result

suggests that consuming photo-excited electrons via the two-electron reduction of O_2 is more efficiently on MW than WO_3. Moreover, the extremely enhanced reduction activity in H_2O_2 generation (12 times) agrees well with the enhanced oxidation activity in photodecomposition of 2-propanol (10 times). The enhancements of both oxidation and reduction activities are believed to be the result of the low charge recombination rate in the MW heterojunction.

The lowered charge recombination rate in MW heterojunction is probably due to the separation of oxidation and reduction sites. In order to distinguish the reduction sites of MW, photocatalytically oxidized methanol on the MW powder using $PtCl_6^-$ as an electron acceptor was carried out [24]. SEM images of WO_3, melamine and MW are showed in Fig. S6. After planetary milling treatment, MW heterojunction shows aggregation of melam and WO_3. TEM image of the MW as shown in Fig. S6d suggests that the WO_3 is partially covered by the melam. This can also be confirmed by high angle annular dark field scanning transmission electron microscopy (HAADF-STEM) and energy-dispersive X-ray spectroscopy (EDS) mapping images, showing that element N and C (belongs to melam) disperse evenly on the WO_3 surface (Fig. S7). As shown in Fig. 4a, small Pt particles (ca. 2 ~ 5 nm) are deposited on the melam, suggesting that the reduction reaction proceeds on the melam in MW. As melam is not a photocatlayst, these results imply that photo-excited electrons are transferred from the conduction band of WO_3 to melam and the electron consumption occurs on melam via the two-electron reduction of O_2 into H_2O_2 (Fig. 4b).

Brunauer-Emmett-Teller (BET) surface area and pore size of the melamine, the WO_3 and the MW were evaluated (Fig. S8 and Table 1). The specific surface area and the pore volume of MW increase 4 times and 6 times as compared to the sum of the melamine and the WO_3, respectively. The increase of the surface area as well as the pore volume is believed to be the result of the

condensation of melamine to melam on the WO_3 during planetary milling treatment. Therefore melam provides not only the charge transfer path but also a larger area of the reduction site. However, 4 times higher specific surface area and 6 times higher pore volume do not match with more than 10 times enhanced photocatalytic activity, which implies the presence of other reason for improving photocatalytic activity.

The aforementioned hydrogen bond N-H···O is believed to play the key role in MW heterojunction. UV-vis diffuse reflectance spectra (DRS) of MW and WO_3 are shown in Fig. S9. Compared with WO_3, the spectrum of MW shows a slight blue shift. It is found that the photo-absorption between 500 - 800 nm of the MW decreases as compared to the WO_3. The photo-absorption in this range is attributed to the appearance of W^{5+} in WO_3, which is due to the electron accumulation in WO_3 ($W^{6+} + e^- \rightarrow W^{5+}$) [17]. The decrease of W^{5+} in the MW is believed to be the result of the transfer electron to the melam. Charge transfer can be further confirmed by XPS, as shown in Fig. 5. The W4f peaks of the MW (37.6 eV and 35.5 eV) shift to higher binding energies as compared to WO_3 (37.4 eV and 35.3 eV). The shift is caused by the electron transfer from WO_3 to melam in the MW sample [31]. Furthermore, the peak of N1s and O1s shifts to the higher (from 398.8 eV to 399.0 eV) and lower (from 530.4 eV to 529.9 eV) binding energy, respectively. These results suggest that electrons are accumulated in the O side and holes are accumulated in N side after forming the N-H···O bonds. As shown in Fig 6, hydrogen bond provides a potential between WO_3 and melam, which drives photo-excited electrons transfer from WO_3 to melam. Moreover, the hydrogen bonds offer a shorter charge transfer route for MW heterojunction. These advantages provided by hydrogen bonds effectively separate photo-excited electrons and holes to lower the recombination rate [32, 33].

The lowered recombination rate can be confirmed by photoelectrochemical measurements. Fig. S10 shows linear sweep voltammetry (LSV) of MW photocathode as well as WO_3 in 0.5 M Na_2SO_4 solution. The onset potential for WO_3 and MW are -0.08 and -0.3 V vs Ag/AgCl, respectively. This clearly indicates that the charge carrier recombination is effectively decreased in MW [34]. The photocurrent of MW is lower than that of WO_3 in the region above 0.03 V because the covering area of MW on FTO is much smaller than that of WO_3, as shown in Fig. S11.

Photoluminescence spectra and the time-resolved fluorescence decay spectra were used to investigate the behavior of photo-excited charge carriers. As shown in Fig. S12a the intensity of MW is stronger than WO_3, which means more charge carriers can be excited under the same incident light source in MW. The signals of 495 nm were chosen to measure the time-resolved fluorescence decay, as shown in Fig. S12b and S12c. The short lifetime (τ_1) of 0.4011 ns in WO_3 increases to 0.4557 ns in MW with its percentage decreases from 97.80% to 90.26%. On the other hand, the long lifetime (τ_2) of charge carriers decreases from 5.9241 ns to 1.8627 ns with its percentage increases from 2.20% to 9.72%. Since the 495 nm is a defect related luminescence, a possible mechanism for the behavior of photo-excited charge carriers is proposed in Fig S13. The increase of τ_1 indicates that the charge carrier recombination is effectively decreased in MW. Moreover, the increase of τ_1 by 0.05 ns and the decrease of τ_2 by 4 ns suggests the existence of an ultrafast path way for charge carrier transfer between WO_3 and melam, which is provided by the hydrogen bond.

In order to determine the stability of MW, repeated consecutive experiment was carried out. Photodecomposition of acetaldehyde was repeated for 3 cycles and the results are shown in Fig. S10. The photocatalytic activity is enhanced in the second cycle, only requires 14 hours for

completely decompose acetaldehyde and the efficiency maintains in the third cycle. The slight improvement of photocatalytic activity is probably due to the increased photo-absorption between 450 – 800 nm (Fig. S11c, UV-vis DRS), which results from the decomposition of free melamine molecules/partial melam after photocatalytic reaction. The XRD and FTIR of samples before and after photodecomposition were also evaluated. No obvious difference can be observed between samples before and after long time photocatalytic reactions (Fig. S11a and S11b). These results imply that the MW heterojunction is stable enough as a photocatalyst in decomposing organic substance in the ambient condition.

Conclusions

In conclusion, visible-light-response heterojunction photocatalyst MW has been synthesized for the first time by facile planetary milling treatment. The low cost MW possesses excellent photocatalytic activities as well as good stabilities. It is demonstrated that Melam and WO_3 are connected by hydrogen bonds, which provide a driven potential and an ultrafast path for photo-excited electrons to separate oxidation and reduction site. Therefore, lower electron-hole recombination rate results in a dramatically enhancement of both oxidation and reduction photocatalytic activities. Not only does melam/WO_3 heterojunction provide an easy way to solve the critical issue of WO_3 as a photocatalyst, but also it offers a promising approach to incorporate melam as an efficient co-catalyst to transition metal oxide photocatalysts.

Acknowledgment

This work was supported by the National Natural Science Foundation of China under Grant No. 51502178, the Shenzhen Science and Technology Project under Grant Nos. JCYJ20150324141711644 and JCYJ20130402151227187 and the Natural Science Foundation of

SZU. Y.J.Z. acknowledges open funding of the State Key Laboratory of Silicon Materials under Grant No. SKL2015-12. H.L. acknowledges funding of China Postdoctoral Science Foundation under Grand No. 2016M590805.

Notes and references

[1] N.S. Lewis, D.G. Nocera, Proc. Natl. Acad. Sci. USA 103 (2006) 15729-15735.
[2] A. Fujishima, K. Honda, Nature 238 (1972) 37-38.
[3] Q. Wang, T. Hisatomi, Q. Jia, H. Tokudome, M. Zhong, C. Wang, Z. Pan, T. Takata, M. Nakabayashi, N. Shibata, Y. Li, I.D. Sharp, A. Kudo, T. Yamada, K. Domen, Nat. Mater. 15 (2016) 611-615.
[4] N. Sagara, S. Kamimura, T. Tsubota, T. Ohno, Appl. Catal. B-Environ. 192 (2016) 193-198.
[5] C. Zeng, Y. Hu, Y. Guo, T. Zhang, F. Dong, X. Du, Y. Zhang, H. Huang, Appl. Catal. B-Environ. 194 (2016) 62-73.
[6] S. Rodrigues, K.T. Ranjit, S. Uma, I.N. Martyanov, K.J. Klabunde, Adv. Mater. 17 (2005) 2467-2471.
[7] O. Tomita, R. Abe, B. Ohtani, Chem.Lett. 40 (2011) 1405-1407.
[8] O. Tomita, T. Otsubo, M. Higashi, B. Ohtani, R. Abe, ACS Catal. 6 (2016) 1134-1144.
[9] D.E. Scaife, Sol. Energy 25 (1980) 41-54.
[10] R. Abe, H. Takami, N. Murakami, B. Ohtani, J. Am. Chem. Soc.130 (2008) 7780-7781.
[11] T. Arai, M. Horiguchi, M. Yanagida, T. Gunji, H. Sugihara, K. Sayama, Chem. Commun. (2008) 5565-5567.
[12] T. Gunji, A.J. Jeevagan, M. Hashimoto, T. Nozawa, T. Tanabe, S. Kaneko, M. Miyauchi, F. Matsumoto, Appl. Catal. B-Environ. 181 (2016) 475-480.
[13] K. Maeda, ACS Catal. 3 (2013) 1486-1503.
[14] L.J. Zhang, S. Li, B.K. Liu, D.J. Wang, T.F. Xie, ACS Catal. 4 (2014) 3724-3729.
[15] Z. Liu, Z.-G. Zhao, M. Miyauchi, J. Phys. Chem. C 113 (2009) 17132-17137.
[16] T. Wang, W. Quan, D. Jiang, L. Chen, D. Li, S. Meng, M. Chen, Chem. Eng. J. 300 (2016) 280-290.
[17] Z. Jin, N. Murakami, T. Tsubota, T. Ohno, Appl. Catal. B-Environ. 150–151 (2014) 479-485.
[18] S.C. Yan, Z.S. Li, Z.G. Zou, Langmuir 25 (2009) 10397-10401.
[19] B.V. Lotsch, W. Schnick, Chem. Eur. J. 13 (2007) 4956-4968.
[20] X.C. Wang, K. Maeda, A. Thomas, K. Takanabe, G. Xin, J.M. Carlsson, K. Domen, M. Antonietti, Nat. Mater. 8 (2009) 76-80.
[21] J. Liu, Y. Liu, N. Liu, Y. Han, X. Zhang, H. Huang, Y. Lifshitz, S.-T. Lee, J. Zhong, Z. Kang, Science 347 (2015) 970-974.
[22] A. Thomas, A. Fischer, F. Goettmann, M. Antonietti, J.-O. Muller, R. Schlogl, J.M. Carlsson, J. Mater. Chem. 18 (2008) 4893-4908.
[23] E. Wirnhier, M.B. Mesch, J. Senker, W. Schnick, Chem. Eur. J. 19 (2013) 2041-2049.
[24] T. Ohno, K. Sarukawa, M. Matsumura, New J. Chem. 26 (2002) 1167-1170.
[25] O. Tomita, B. Ohtani, R. Abe, Catal. Sci. Technol. 4 (2014) 3850-3860.

[26] L.V.C. Lima, M. Rodriguez, V.A.A. Freitas, T.E. Souza, A.E.H. Machado, A.O.T. Patrocínio, J.D. Fabris, L.C.A. Oliveira, M.C. Pereira, Appl. Catal. B-Environ. 165 (2015) 579-588.
[27] A. Lautié, F. Froment, A. Novak, Spectrosc. Lett. 9 (1976) 289-299.
[28] P. Gilli, V. Bertolasi, V. Ferretti, G. Gilli, J. Am. Chem. Soc. 122 (2000) 10405-10417.
[29] L. Yu, R. Zou, Z. Zhang, G. Song, Z. Chen, J. Yang, J. Hu, Chem. Commun. 47 (2011) 10719-10721.
[30] T. Arai, M. Horiguchi, M. Yanagida, T. Gunji, H. Sugihara, K. Sayama, J. Phys. Chem. C 113 (2009) 6602-6609.
[31] Z. Liu, Z.-G. Zhao, M. Miyauchi, J. Phys. Chem. C 113 (2009) 17132-17137.
[32] D.R. Weinberg, C.J. Gagliardi, J.F. Hull, C.F. Murphy, C.A. Kent, B.C. Westlake, A. Paul, D.H. Ess, D.G. McCafferty, T.J. Meyer, Chem. Rev. 112 (2012) 4016-4093.
[33] M.D. Ward, Chem. Soc. Rev. 26 (1997) 365-375.
[34] J.A. Seabold, K.-S. Choi, Chem. Mater. 23 (2011) 1105-1112.

Figure captions

Fig. 1 (a) XRD patterns of WO_3, MW and melamine. For clarity, the intensity of melamine is divided by 10. (b) FTIR reflectance of WO_3, MW and melamine, (inset) 800 – 1100 cm^{-1} FTIR reflectance of WO_3 and MW.

Fig. 2 Route of synthesis of melam/WO_3 by planetary milling treatment.

Fig. 3 (a) Time courses of CO_2 liberation from acetaldehyde decomposition; (b) An action spectrum with UV-vis absorption spectra of MW; (c) Acetone liberation from 2-propanol over WO_3 and MW under 435-nm LED irradiation (3 mW cm^{-2}); (d) Time courses of H_2O_2 liberation in the pure water.

Fig. 4 (a) TEM image of Pt loaded MW; (b) The proposed mechanism of loading Pt on WO_3.

Fig. 5 XPS spectra of WO_3, melamine, and MW. (a) Survey scan; (b) W4f; (c) N1s; (d) O1s.

Fig. 6 Proposed mechanism of electron transfer via the hydrogen bonding in the Melam/WO_3 nanocomposite.

Table 1 BET specific surface area and pore distributions of WO_3, melamine, and MW.

Graphical abstract

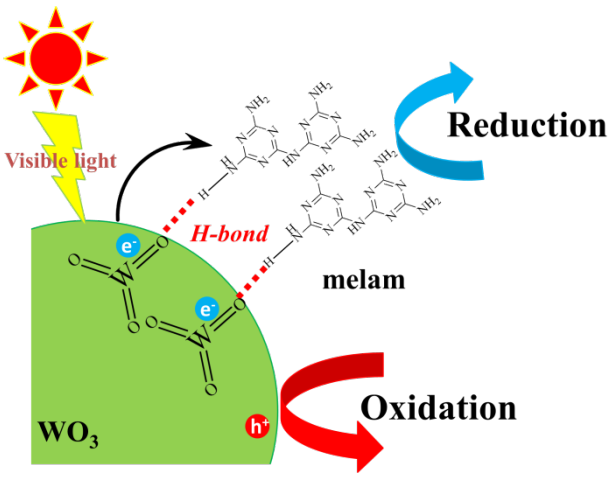

Figure 1

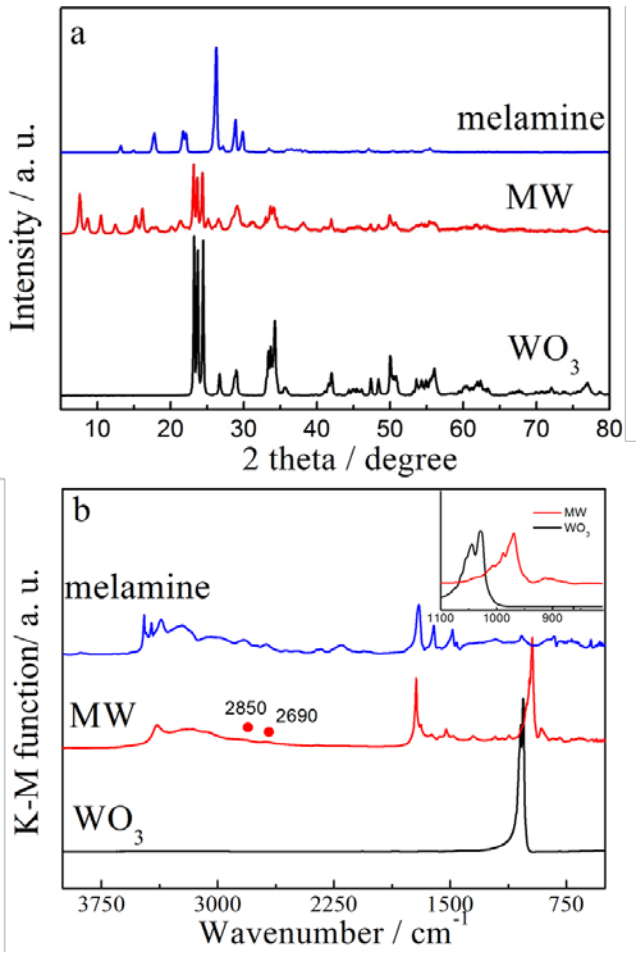
a
melamine
MW
WO3
Intensity / a. u.
10
20
30
40
50
60
70
80
2 theta / degree
b
melamine
MW
WO3
2850
2690
MW
WO3
1100
1000
900
K-M function/ a. u.
3750
3000
2250
1500
750
Wavenumber / cm-1

Figure 2

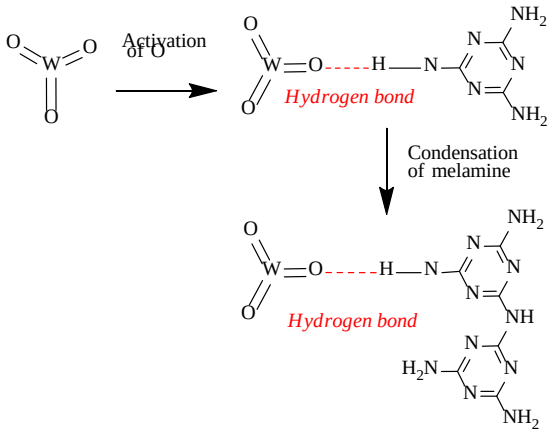
Activation
of O
Hydrogen bond
Condensation
of melamine
Hydrogen bond

Figure 3

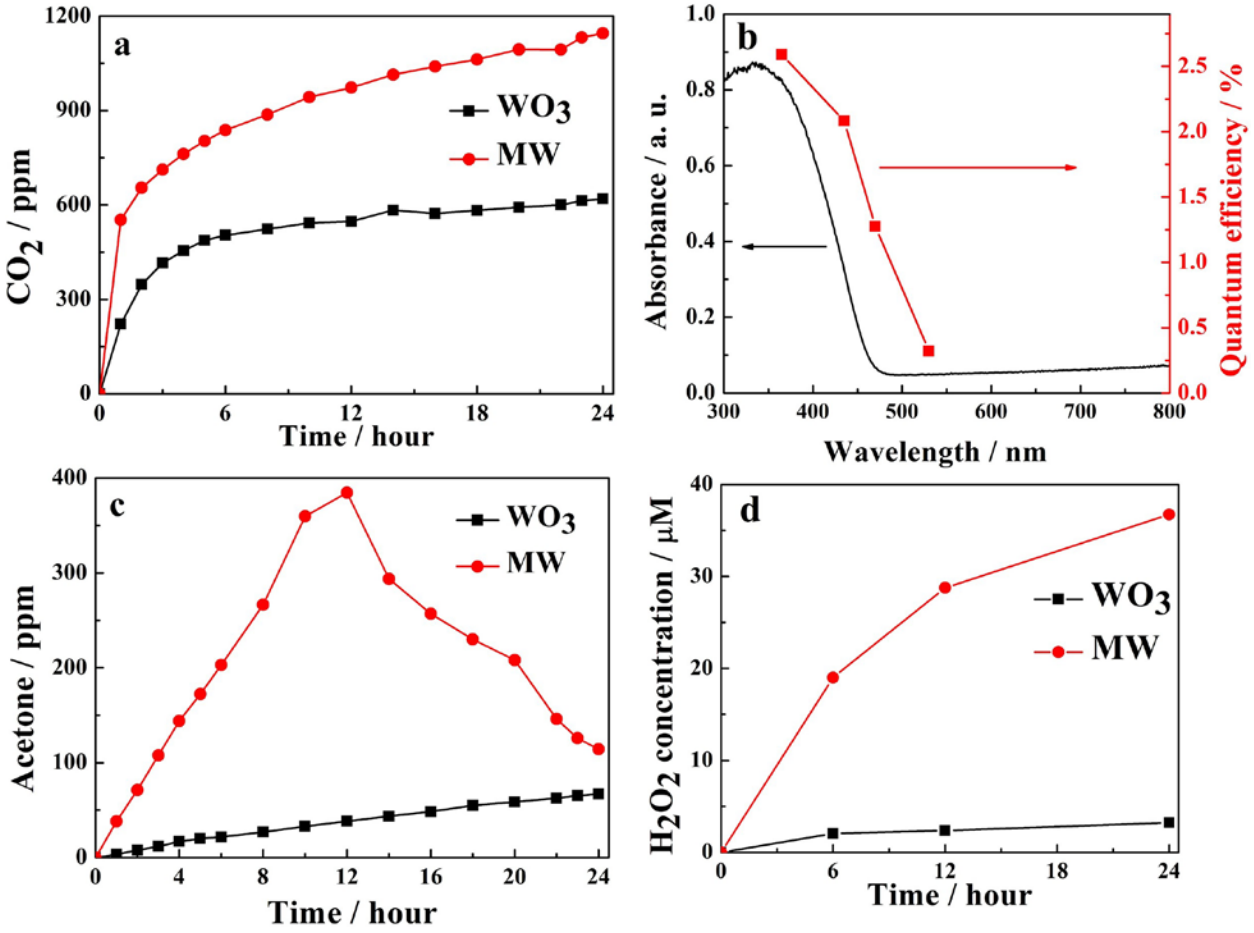
a
CO_2 / ppm
Time / hour
WO_3
MW
b
Absorbance / a. u.
Quantum efficiency / %
Wavelength / nm
c
Acetone / ppm
Time / hour
WO_3
MW
d
H_2O_2 concentration / μM
Time / hour
WO_3
MW

Figure 4

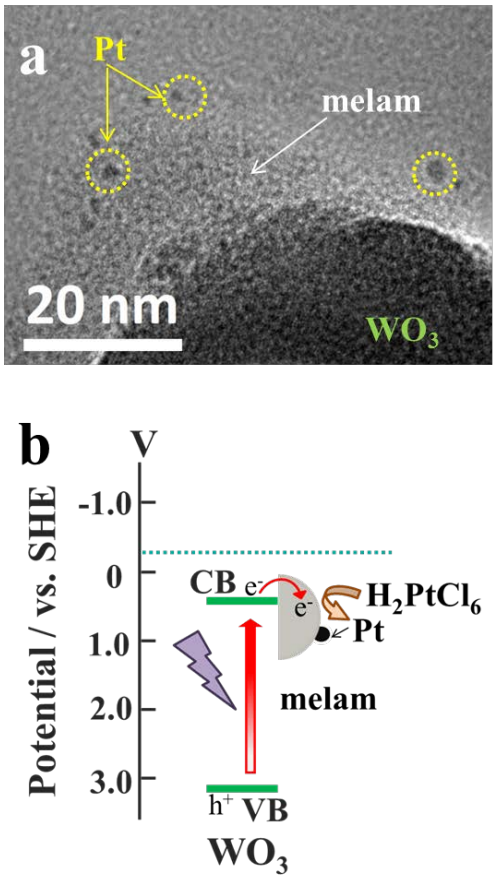
a
Pt
melam
20 nm
WO3
b
V
-1.0
0
1.0
2.0
3.0
Potential / vs. SHE
CB e-
e-
H2PtCl6
Pt
melam
h+ VB
WO3

Figure 5

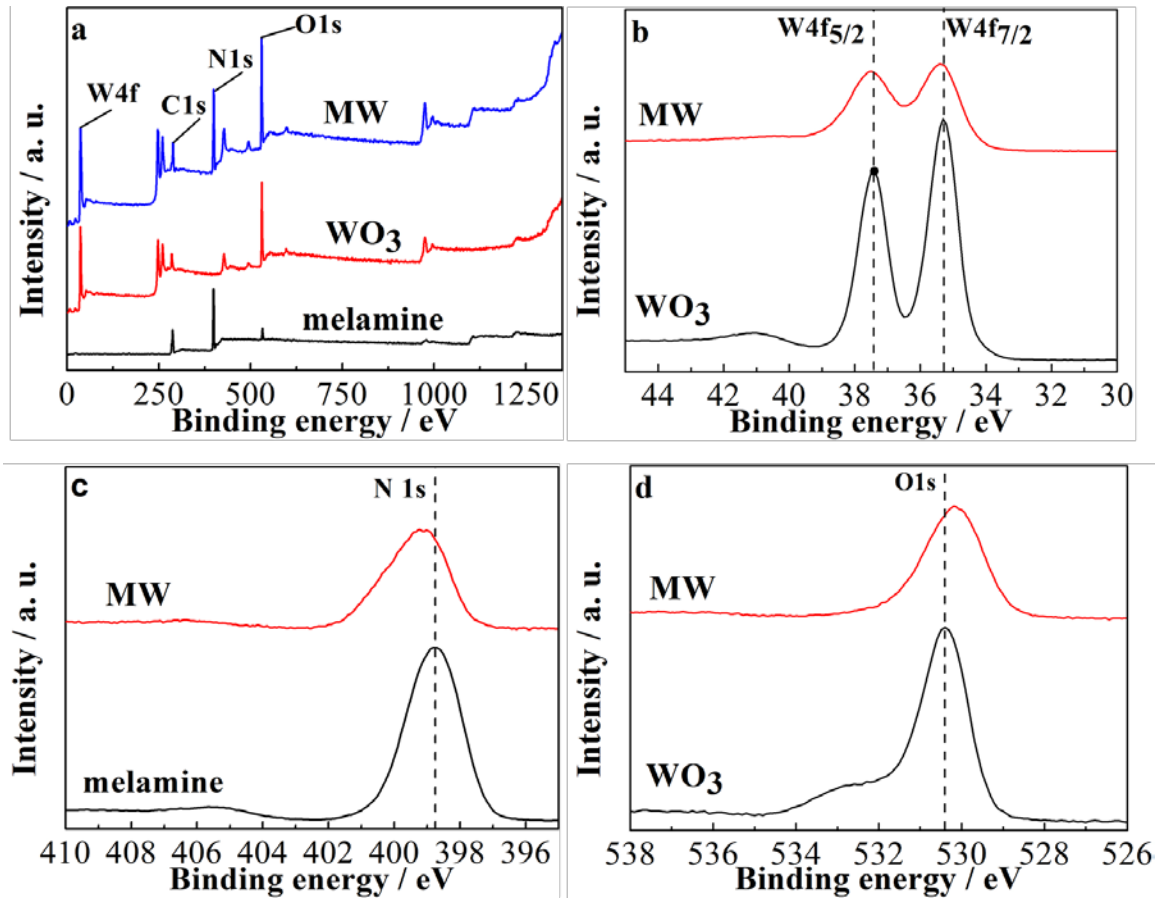
a
O1s
N1s
W4f
C1s
MW
WO3
melamine
Intensity / a. u.
0 250 500 750 1000 1250
Binding energy / eV
b
W4f5/2
W4f7/2
MW
WO3
Intensity / a. u.
44 42 40 38 36 34 32 30
Binding energy / eV
c
N 1s
MW
melamine
Intensity / a. u.
410 408 406 404 402 400 398 396
Binding energy / eV
d
O1s
MW
WO3
Intensity / a. u.
538 536 534 532 530 528 526
Binding energy / eV

Figure 6

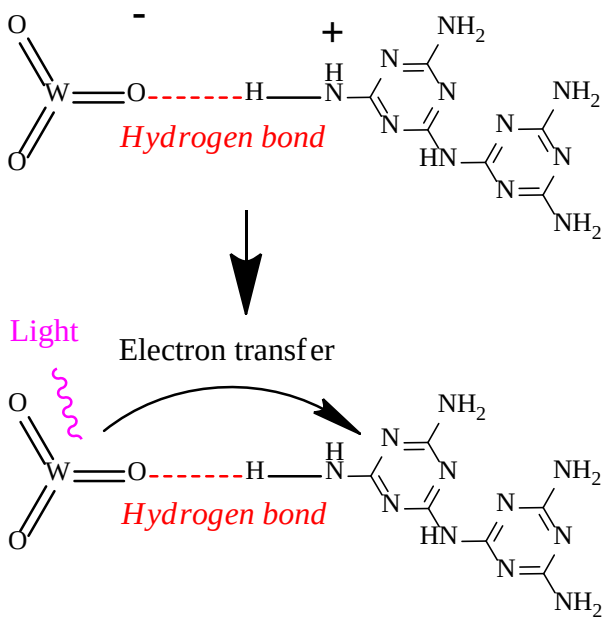

Table 1

	Specific surface area (m^2/g)	Pore diameter (nm)	Pore volume (cm^3/g)
WO_3	5.95	1.65	0.008
Melamine	1.69	2.39	0.002
MW	24.15	1.64	0.065